Journal of Applied Polymer Science

Poly(styrene-*co*-maleic anhydride) Ionomers as Nucleating Agent on the Crystallization Behavior of Poly(ethylene terephthalate)

Shili Xing, Ping Tang, Yuliang Yang
State Key Laboratory of Molecular Engineering of Polymers, Department of Macromolecular Science, Fudan University, Shanghai 200433, China
Correspondence to: P. Tang (E-mail: pingtang@fudan.edu.cn)

ABSTRACT: Poly(styrene-*co*-maleic anhydride) (SMA) ionomers were synthesized and designed as a new kind of nucleation agent according to the crystallization theory for improving the crystallization of poly(ethylene terephthalate) (PET). The crystallization behavior of PET with the addition of nucleation agents was investigated by differential scanning calorimetry, polarized-light microscope, and X-ray diffraction (XRD). Avrami equation and Hoffman–Lauritzen theory are adopted for analyzing isothermal and non-isothermal crystallization kinetics, respectively. The results show that the addition of 1 wt % SMA ionomers effectively accelerates the crystallization rate and reduces the fold surface free energy of PET at high temperature regions. PLM results also indicated that the crystals impinge on each other, thus decreasing the spherulite size for PET/SMA ionomers samples compared with PET. XRD measurement revealed that the introduction of SMA ionomers does not change the crystal structure but indeed accelerates the crystallinity of PET. The results clearly demonstrate that our synthesized SMA ionomers are an efficient nucleating agent for PET. © 2014 Wiley Periodicals, Inc. J. Appl. Polym. Sci. **2015**, *132*, 41240.

KEYWORDS: crystallization; interfaces; polyesters; surfaces

Received 15 January 2014; accepted 29 June 2014
DOI: 10.1002/app.41240

INTRODUCTION

Studies related to the melting and crystallization behaviors of semicrystalline polymers are of great importance in engineering polymeric materials such as plastic molding and fiber spinning. The resulting physical and mechanical properties of the products strongly depend on the extent of the crystallization and crystal morphologies. Poly(ethylene terephthalate) (PET) is a typical linear semicrystalline thermoplastic polyester with excellent mechanical, physical, and chemical properties especially low cost. However, one of the major drawbacks of PET is the rather slow crystallization rate and high crystallization temperature resulting in high mold temperature in injection molding processing, thus limiting its commercial utilization especially as engineering plastics. Most study in this field has been focused on the way of increasing the crystallization rate and decreasing crystallization supercooling degree.[1–12]

Nucleation agents and nucleation promoting agents have been introduced to improve the nucleation efficiency thus accelerating the crystallization rate by providing more nucleation sites with the surface for easy crystal growth.[13] In general, not only can nucleation agents direct the development of a given crystalline polymorph, but also have a strong influence on the overall crystallization kinetics, the spherulite size, and its distribution and the physical properties of final products.[9,14] Now a lot of study reported that the addition of the nucleation agents to polymer matrix is one of the most efficient methods to improve the crystallization rate of PET.[1,15–17] Nucleation agents are usually low molecular weight organic and inorganic compounds. Inorganic nucleating agents can behave as heterogeneous substrates in lowering the energy barrier for crystal nucleation, but the problem of compatibility and dispersion abilities is difficult to solve. Organic nucleating agents can dissolve in the polymer and react with the molten macromolecules to form homogeneous system, which cannot provide a large number of interfaces for crystallization and crystal growth. According to the crystallization theory, these requirements are necessary for designing effective nucleation agents. First of all, nucleation agents should have good compatibility with polymer matrix when melt blending.[18,19] Secondly, effective nucleating agents should be solid phase and have good thermal stability at the crystallization temperature of polymers. Furthermore, nucleation agents can provide more interfaces for polymer crystallization.[20,21] In this regard, metal salts of polymers, named ionomers, can server in this role,[17,22,23] and reduce the degree of supercooling of polymers by increasing the onset of crystallization temperature. In fact, ionomers have been used as nucleation agents to increase the crystallization rate of PET, such as ethylene-sodium methacrylate

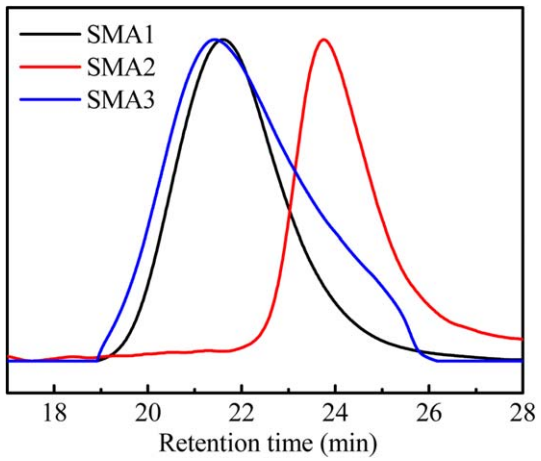

Figure 1. GPC curves of SMA copolymers. [Color figure can be viewed in the online issue, which is available at wileyonlinelibrary.com.]

copolymers (trade name Surlyn),[24] ethylene-sodium acrylate copolymers (trade name AClyn),[25,26] poly(styrene-*block*-acrylate-kalium) copolymers.[27] However, Berti et al.[28] reported the crystallization rate of PET decreased with the ionic group (—SO_3Na) content by blending sodium salt of *n*-butyl-2-sulfobenzoate (2-SBABE) ionomers with PET. In contrast, the ionomers containing carboxylate played an effective role in acting as nucleation agents for PET due to the reaction of carboxylate and PET chain end. Therefore, the good compatibility between the nucleation agent and PET matrix is one of the most important factors to design effective nucleation agents. Maleic anhydride (MA) copolymers or grated polymers are often used to improve the compatibility of PET with polymers. For instance, the effect of MA grafted linear low-density polyethylene (LLDPE-*g*-MA) on thermal properties and morphology of recycled PET was studied by Zhang et al.[29] The results showed that lower LLDPE-*g*-MA content benefited the formation of PET crystal cell on the interface. However, crystallinity of PET decreased with the increase of LLDPE-*g*-MA content because PET-*co*-LLDPE-*g*-MA copolymers might destroy regular structure of PET chain thus restricting PET chain from entering into crystal cells. Yoon et al.[30] investigated the properties of PET and PP-*g*-MA reactive blends and found that MA improves the compatibility between PP and PET. They also reported the effect of the addition of poly(styrene-*co*-maleic anhydride) (SMA) on the rheology, morphology, and mechanical properties of blends of PET and SMA due to the improved miscibility of PET with SMA.[31] Unfortunately, the crystallization behavior was not reported.

Based on this, we try to design a new kind of nucleation agent, which not only has a good compatibility with PET matrix but also can easily be made into ionomers. To confirm our idea, we aim at studying the effect of SMA ionomers with different molecular weights and ratios between the monomer MA and styrene on the crystallization behaviors of PET.

EXPERIMENTAL

Materials

PET with intrinsic viscosity of 0.9 dL/g was produced by Sinopec Yizheng Chemical Fiber Company Limited, China. Commercialized SMA random copolymer (trade name SE26080), denoted by SMA1 was purchased from Polyscope, The Netherlands. We synthesized SMA with different molecular weights named SMA2 and SMA3, with free radical polymerization in cyclohexanone with benzoyl peroxide (BPO) as initiator. All of these three types of SMA copolymers were dissolved in tetrahydrofuran (THF) and poured dropwise into methanol and this process was repeated at least three times in order to purify the SMAs. The SMAs were further purified with Soxhlet extraction method with toluene as the solvent for at least 24 hours in order to remove the unreacted monomers and a small amount of polystyrene homopolymer. MA and BPO were purchased from Alfa Aesar and recrystallized three times from chloroform. Styrene (St) and cyclohexanone were obtained from Sinopharm Chemical Reagent Co., Ltd and redistilled to remove water and inhibitor. Other chemicals were purchased from the Sinopharm Chemical Reagent Co., Ltd and all of them were analytical grade and used without further purification.

Preparation of Ionomers and PET/Ionomers Blends and Characterization of Ionomers

Firstly, methanol solution of sodium hydroxide was added dropwise into SMA copolymer solution of dioxane (0.1 g/mL) at room temperature and SMA ionomers were precipitated from the solution. Then the precipitated ionomers were dissolved in methanol again and precipitated in toluene, repeating this treatment at least three times to ensure removing the additional sodium hydroxide. The final products were dried at 60°C in the vacuum oven for 24 hours. PET was dried at 110°C for 24 hours in the vacuum oven prior to use to prevent hydrolysis during the processing. Then PET was mixed with 1 wt % SMA ionomers in the Kechuang XSS-300 torque rheometer made in China at 280°C with twin-screw speed of 80 rpm for 5 min in an internal batch mixer for further study. All the samples were quenched in iced water when taken from the rheometer.

The molecular weight and polydispersity index (PDI) of the prepared SMA copolymers were determined by a gel permeation chromatography (GPC) with THF as solvent at a flow rate of 1.0 mL/min at room temperature on HP 1100 with a series of columns (Phenogel 100 A, Phenogel 100 KA, Phenogel mix) using refractive index (RI) and ultraviolet (UV) detectors. The injection volume was 20 μL of 0.5% copolymers in THF. The molecular weight and PDI were based on a linear calibration curve constructed with polystyrene standards with low polydispersity (M_n = 800, 2000, 4000, 9000, 30,000, 50,000, 100,900, and 233,000). GPC curves are shown in Figure 1 with extracted values listed in Table I.

Fourier transform-infrared (FTIR) spectra were recorded on a Nicolet 6700 with DTGS detector at wavenumbers between 400 and 4000/cm and with 64 scans being taken at 4/cm resolution. Element analysis for C, H, and O was carried on the VarioEL-III element analyzer. ^{13}C NMR and ^{1}H NMR spectra were

Table I. The Molecular Weight and PDI of SMA Copolymers

	SMA1	SMA2	SMA3
M_n (g/mol)	39,100	13,300	31,050
M_w (g/mol)	66,100	16,800	56,960
PDI	1.69	1.26	1.83

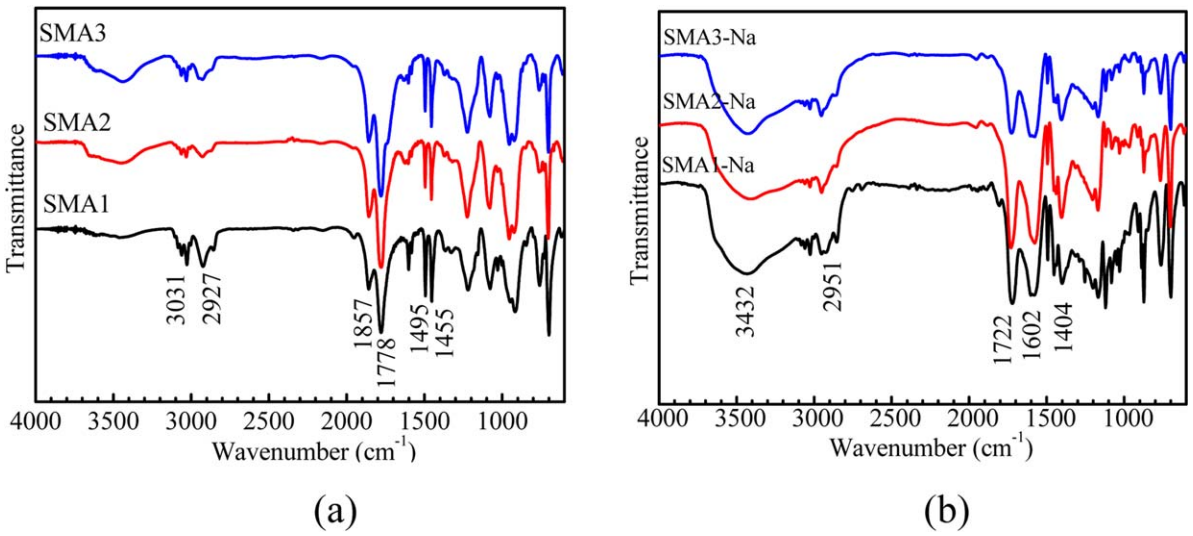

Figure 2. FTIR spectra of SMA (**a**) and its ionomers (**b**). [Color figure can be viewed in the online issue, which is available at wileyonlinelibrary.com.]

recorded on Bruker DMX 500 MHz at 25°C with acetone-d_6 as solvent at a resonance frequency of 500 MHz to study the ratio of MA to styrene and sequence distribution. For the analysis of sequence distribution, overlapping peaks were integrated after Lorentzian deconvolution of the spectra using the deconvolution option implemented in the MestReNova NMR-software. The thermal stability behavior of SMA ionomers was investigated by TA thermogravimetric analyzer (TGA) Q5000 instrument at the heating rate of 20°C/min from room temperature to 700°C in the nitrogen atmosphere.

Crystallization Behavior Measurements

The isothermal and non-isothermal crystallization behaviors of PET-based samples were investigated by differential scanning calorimetry (DSC) in a TA instruments DSC-Q2000 in the nitrogen atmosphere. To investigate the isothermal melt-crystallization and melting behavior, the samples with 3–5 mg were heated to 280°C rapidly and maintained for 5 min to erase the previous thermal history under the standard mode for DSC, then cooled to the target crystallization temperature T_c at a rate of 200°C/min and maintained at that temperature for at least 60 min for completing crystallization of the samples. The enthalpy evolved during the isothermal crystallization was recorded as a function of time at different T_c. The samples were subsequently heated to 280°C at a heating rate of 10°C/min to obtain the corresponding melting behavior. The values of melting temperature T_m and enthalpy of fusion ΔH_f of the samples were calculated from the peak temperature and the area under the endothermic peak, respectively. To investigate the non-isothermal crystallization, the samples also needed to erase the

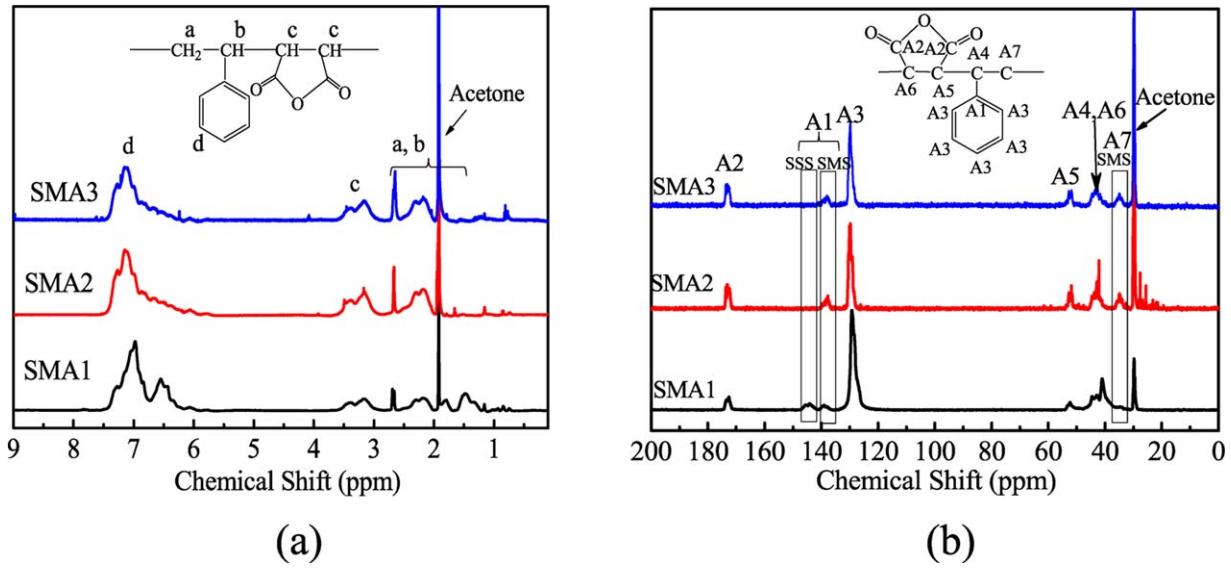

Figure 3. NMR spectra of SMAs with peak assignments: (**a**) ^{1}H NMR; (**b**) ^{13}C NMR. [Color figure can be viewed in the online issue, which is available at wileyonlinelibrary.com.]

Table II. Element Analysis Results of SMA

	C (wt %)	H (wt %)	O (wt %)	Mole ratio[a]	Mole ratio[b]
SMA1	81.1	5.9	12.6	2.71 : 1	3.16 : 1
SMA2	70.9	4.8	24.1	0.97 : 1	1.08 : 1
SMA3	70.1	4.9	24.7	0.92 : 1	1.12 : 1

Mole ratio[a]: mole ratio of styrene to MA calculated by element analysis; Mole ratio[b]: mole ratio of styrene to MA calculated by ^{1}H NMR.

previous thermal history and then cooled at various rates from 280°C to 50°C in order to observe non-isothermal melt-crystallization behavior (cooling curve). The data of DSC were analyzed by TA universal analysis software.

The polarized-light microscope (PLM) from Olympus with a hot stage (model THMS-600, Linkam, United Kingdom) and video camera was used to investigate the crystallization morphology. The samples were sandwiched between two microscope cover slips and placed on the hot stage under the nitrogen atmosphere. Next, the samples were rapidly heated to 280°C with a heating rate of 100°C/min and pressed to a thin film with a thickness of approximate 10 μm and held there at 280°C for 5 min to erase the previous thermal history. Then the film was rapidly quenched at a cooling rate of 130°C/min to T_c and maintained at that temperature for completing crystallization of the samples. The growth of spherulites as a function of time was recorded by a CCD camera.

X-ray diffraction (XRD) analysis was performed with the X'Pert PRO model (PANalytical B.V., The Netherlands) wide-angle X-ray diffractometer with a Cu anode, running at 40 kV and 40 mA, scanning from 5° to 60° at 3°/min. The samples used in XRD analysis were compression-molded with two silicon wafers at 280°C in a glove box to isolate water and oxygen then the covered silicon wafers were peeled off. The thickness of samples were approximately 10 μm. All samples needed to be held at 280°C for 5 min to erase the previous thermal history and then quenched into liquid nitrogen to get the amorphous samples. The amorphous samples were used to do the XRD analysis firstly. After that, the amorphous samples were rapidly moved to heating stage at 220°C for at least 2 min for isothermal crystallization and then quenched into liquid nitrogen. For comparison, PET sample was further hold at 220°C for 60 min in order to obtain the fully crystallized sample and then quenched into liquid nitrogen.

RESULTS AND DISCUSSION

Synthesis and Characterization of SMA and its Ionomers

MA itself does not homopolymerize and the reactivity ratio between St and MA is r_1=0.04 (ratio of St homopolymerization rate to St/MA copolymerization) and r_2=0.015 (ratio of MA homopolymerization rate to St/MA copolymerization) in the free radical polymerization. Therefore, MA copolymerization with St has a strong tendency toward alternation especially under the feed mole ratio of styrene and MA of 1 :1.2 in our experiments. These copolymers therefore need to be purified with Soxhlet extraction method by toluene for at least 24 hours in order to remove the unreacted monomers and a small amount of polystyrene homopolymer.

From FTIR spectra of SMA polymers shown in Figure 2(a), the strong absorption peaks at 1778 and 1857 cm^{-1} are characteristics of the anhydride.[32] The peaks at 1455and 1495 cm^{-1} correspond to phenyl ring. The peaks at 2927 and 3031 cm^{-1} are assigned to the absorption of methylene and methine on the polymer chain. Therefore, it is confirmed that the poly(styrene-*alt*-maleic anhydride) copolymers have been synthesized successfully. The FTIR spectra of SMA ionomers in Figure 2(b) show a strong absorption at 3432 cm^{-1} assigned to the absorption of carboxylate. Moreover, peaks corresponding to the structure of SMA are blue-shifted slightly due to the salinization effect.

The element analysis and ^{1}H NMR measurements were used to calculate the mole ratio between MA and styrene. We assume that the mole ratio of styrene to MA is x : 1, which can be calculated by eq. (1) based on the element analysis and eq. (2) based on the ^{1}H NMR spectra shown in Figure 3(a). The chemical shift of protons in CH_2, CH, and benzene ring was marked in the spectra, mainly referring to the literature.[33] The mole ratio of St and MA can be calculated based on the integrated area under corresponding peaks of proton H_c and H_d. The ratios of integrated area of corresponding peaks of proton H_c and H_d for the three SMA copolymers are 1 : 7.9, 1 : 2.7, and 1 : 2.8, respectively. The calculated results are concluded in Table II. The mole ratio between MA and styrene of SMA1 is about 1 : 3, while the mole ratios between MA and styrene of SMA2 and SMA3 are about 1 : 1. The mole ratios by the two measurements are almost consistent.

$$\frac{(8x+4)\times 12}{16\times 3} = \frac{\mathrm{C(wt\ \%)}}{\mathrm{O(wt\ \%)}} \quad (1)$$

$$\frac{2}{5x} = \frac{\text{Integrated area}_{(H_c)}}{\text{Integrated area}_{(H_d)}} \quad (2)$$

Figure 3(b) shows ^{13}C NMR spectra of SMA with structural assignments, mainly referring to the literature.[34–36] The chemical shift of characteristic carbons in MA and styrene was

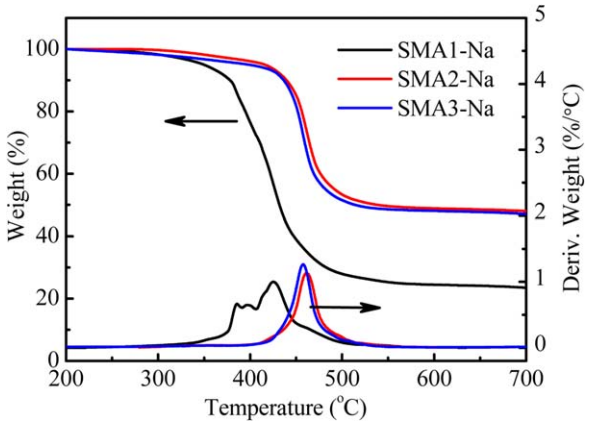

Figure 4. TGA and their differential curves of SMA ionomers. [Color figure can be viewed in the online issue, which is available at wileyonlinelibrary.com.]

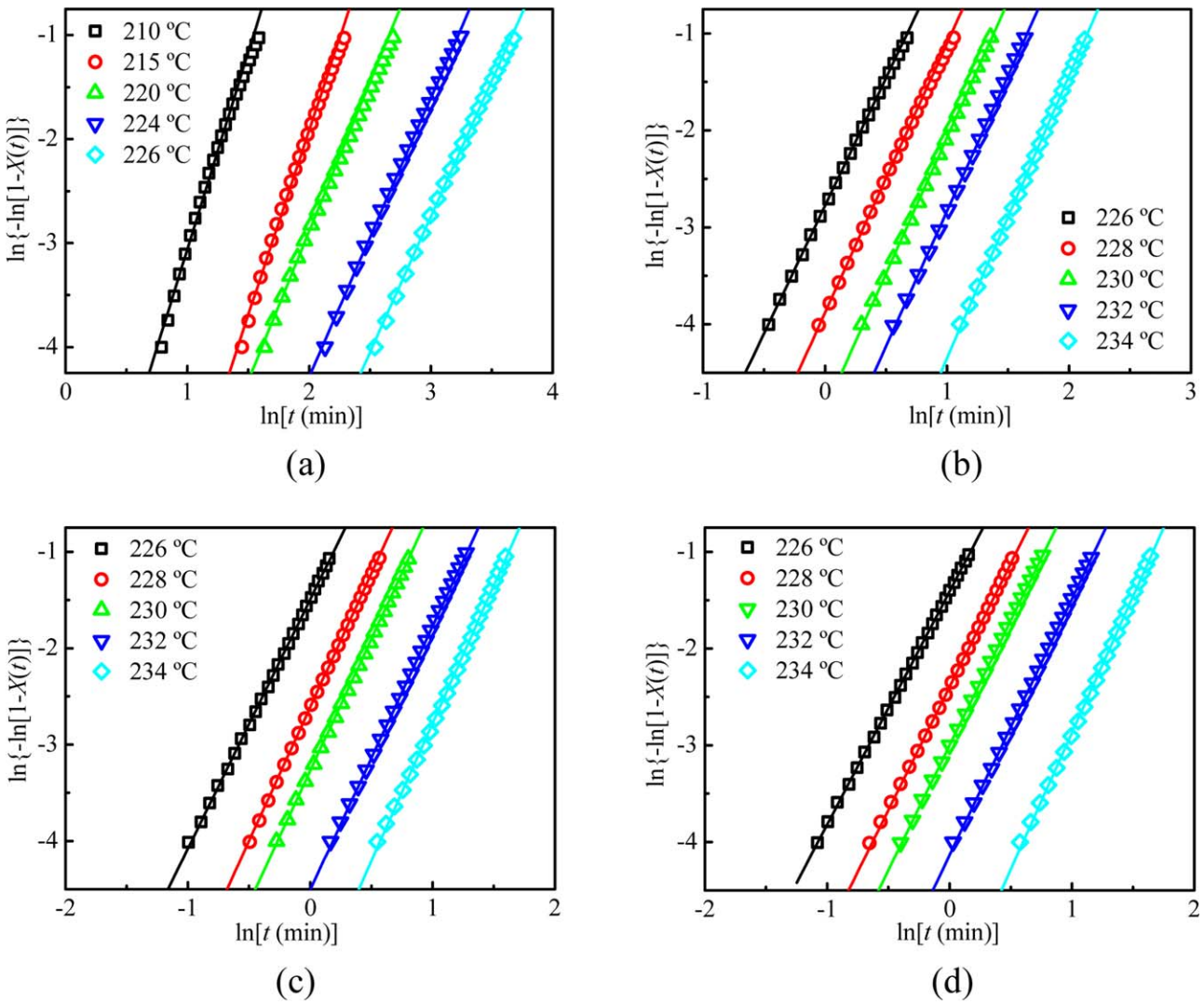

Figure 5. Plots of $\ln\{-\ln[1-X(t)]\}$ versus $\ln t$ for isothermal crystallization with each curve showing only the linear portion. (**a**) PET; (**b**) PET/SMA1-Na; (**c**) PET/SMA2-Na; (**d**) PET/SMA3-Na. [Color figure can be viewed in the online issue, which is available at wileyonlinelibrary.com.]

marked in the spectrum. The chemical shift of carbon of C═O in MA appears at about 173 ppm, that of No. 1 and No. 7 carbons in styrene appears at about 140 and 35 ppm, respectively. From Figure 3(b), the peak at 140 ppm for SMA1 is quite clearly separated into two peaks, and the resonance of No. 7 carbon corresponding to alternating copolymer is relatively weak. All of these evidences reflect that SMA1 is a random copolymer. In contrast, there is only one peak at 140 ppm and there is a clear resonance of No. 7 carbon for SMA2 and SMA3. Therefore, we conclude that the monomer sequence distribution for SMA2 and SMA3 should be alternating copolymers.

Thermal Stability Behavior of SMA Ionomers

Figure 4 shows the TGA and their differential curves of the SMA ionomers. All the degradation temperature was measured from the thermogram curve by onset extrapolation. It is clear that the degradation temperature of these three ionomers is above 300°C, suggesting that the ionomers remain the solid states without degradation thus providing nucleating sites around which the PET spherulites can form. The anhydride of SMA has been salinized by sodium hydroxide and cannot been degraded, which leads to the different residues among the SMA ionomers. Furthermore, sodium anhydride can directly react with PET,[29] resulting in the formation of the clusters between ionomers and the functional groups of PET chain end.[25] Therefore, the interactions of SMA ionomers with PET chain might provide heterogeneous nucleus sites and decrease the fold surface free energy at the crystallization process of PET, as discussed in the following DSC measurements.

Isothermal Crystallization Behavior of PET and PET/SMA Ionomers

The crystal growth process can be influenced or even controlled by the nucleation behavior, necessitating to distinguish the nucleation type in the crystallization process. For most cases of interest, isothermal crystallization can be used to describe the

Table III. Parameters of Isothermal Crystallization from Avrami Equation

Samples	T_c(°C)	$\ln K_t$	n	$t_{1/2}$(s)
PET	210	−6.85	3.79	332
	220	−8.63	2.87	1067
	226	−10.58	2.60	2996
PET/SMA1-Na	226	−2.78	2.60	151
	230	−4.89	2.80	299
	234	−7.27	2.90	639
PET/SMA2-Na	226	−1.49	2.58	93
	230	−3.27	2.74	173
	234	−5.63	2.85	380
PET/SMA3-Na	226	−1.41	2.40	93
	230	−3.01	2.58	167
	234	−5.69	2.83	396

nucleation type and growth rate. Although many methods and theories were used to study the isothermal crystallization, the Avrami analysis has been the most widely applied approach to describe the information, such as analyzing the nucleation mechanism, comparing the crystallization rate of polymers. Equation (3) is commonly termed as the Avrami equation:[37,38]

$$\ln\{-\ln[1-X(t)]\}=n\ln t+\ln K_t \quad (3)$$

where $X(t)$ is the relative crystallinity at different crystallization time. The exponent n is usually termed as Avrami exponent, which is influenced by the molecular weight,[39] nucleation type,[40] secondary crystallization,[41] and has a weak relationship with the temperature.[42] From a graphic representation of $\ln\{-\ln[1-X(t)]\}$ versus $\ln t$ according to eq. (3), n is valued as the slope of the straight line and the natural logarithm of crystallization kinetic constant $\ln K_t$ as the intercept. In the induction period of crystallization, the crystal nuclei are unstable and during the later stage of crystallization the impingement of two adjacent growing centers causes a cessation of their growth. The both cases lead to some deviation from normal Avrami theory. Therefore, the area of $X(t)$ from 0.02 till 0.3 was selected to be applied in the Avrami equation for PET crystallization in this article. The crystallization rate of polymer can also be characterized by the half-time of crystallization $t_{1/2}$, which is defined as the time taken from the onset of the relative crystallization until 50% completion in the isothermal crystallization process. The $t_{1/2}$ can be calculated from eq. (4).

$$t_{1/2}=(\ln 2/K_t)^{1/n} \quad (4)$$

Thus, $t_{1/2}$ is related to K_t and n. In order to analyze the effect of temperature on the crystallization behavior, plots of $\ln\{-\ln[1-X(t)]\}$ versus $\ln t$ at different crystallization temperatures are shown in Figure 5 and the related parameters extracted from Figure 5 are summarized in Table III.

It is observed that the crystallization shifted to longer time with increasing in the crystallization temperature both for PET and PET with the addition of SMA ionomers. For neat PET, $t_{1/2}$ increases 73 and 321 s each degree rise in T_c for $T_c = 210$°C–220°C and $T_c = 220$°C–226°C, respectively. In contrast, for PET/SMA1-Na, $t_{1/2}$ increases 36 and 85 s each degree rise in T_c for $T_c = 226$°C–230°C and $T_c = 230$°C–234°C, respectively. Therefore, the neat PET crystallization is more sensitive to the crystallization temperature than that of PET/SMA ionomers, because PET needs larger supercooling degree to trigger the chain orientation. From Table III, it is clear that the intercept value $\ln K_t$ decreases with increasing isothermal crystallization temperature. Moreover, $\ln K_t$ of PET/ SMA ionomers is larger than that of PET even if the isothermal crystallization temperature is 20°C higher than that of PET. Besides, the $t_{1/2}$ of PET/SMA ionomers samples in isothermal crystallization is shorter than that of PET. As discussed later, this is related to the difference in the crystallization process for PET and PET/SMA ionomers blends. The crystallization of PET/SMA ionomers proceeds mainly via heterogeneous nucleation and the number of heterogeneous nuclei in PET/SMA ionomers due to the addition of SMA ionomers is much larger than that in PET while PET proceeds by both heterogeneous and homogeneous nucleation mechanisms. Therefore, SMA ionomers can increase the crystallization rate of PET. Furthermore, there is another important trend reflected from Figure 5 and Table III. The crystallization rate constants K_t gradually increase from SMA1 to SMA2 and SMA3 ionomers at the same crystallization temperature and the crystallization half-time is shorter with this trend. These results indicate that the nucleation effect of SMA ionomers is strengthened with increasing the content of MA in SMA copolymers because SMAs with more content of MA have better compatibility with PET matrix. Therefore, the good compatibility of nucleation agents with PET matrix is of great importance to act as nucleation agents. Furthermore the nucleation effect of SMA ionomers is slightly influenced by the molecular weight and PDI of SMA copolymers. SMA ionomers with higher molecular weights do not improve the nucleation process and the effect is not obvious, which will also be discussed in the following part of non-isothermal crystallization process. Polymer chain needs larger supercooling degree to trigger the orientation. Therefore, it is difficult for PET chain to undergo three-dimensional (3D) growth at higher temperatures. But for PET/SMA ionomers samples, the orientation of polymer chains can be accelerated by the nucleation agents at higher temperatures thus tending to 3D growth.

Figure 6 shows optical micrographs taken at various isothermal crystallization temperatures to investigate time-dependent spherulite growth with the initial melt conditions. The spherulite size increases with the time evolution for isothermal crystallization at 220°C for both PET in Figure 6(a–d) and PET/SMA ionomers in Figure 6(i–k), respectively, and at 230°C for PET in Figure 6(e–f). For PET, the crystal stopped growing until 300, 420, and 180 s for isothermal crystallization at 220°C, 230°C and at 210°C and 215°C, respectively; while for PET/SMA ionomers, the crystal stopped growing about at 90 s at 220°C, indicating that SMA ionomers indeed accelerate the crystallization rate of PET. We note that the observed crystallization time is about 30 min for each temperature and the pictures (not shown here) are almost the same as the final phase pictures shown in Figure 6. From Figure 6, the spherulite grows slowly with temperature increasing. Moreover, the nucleation density decreases

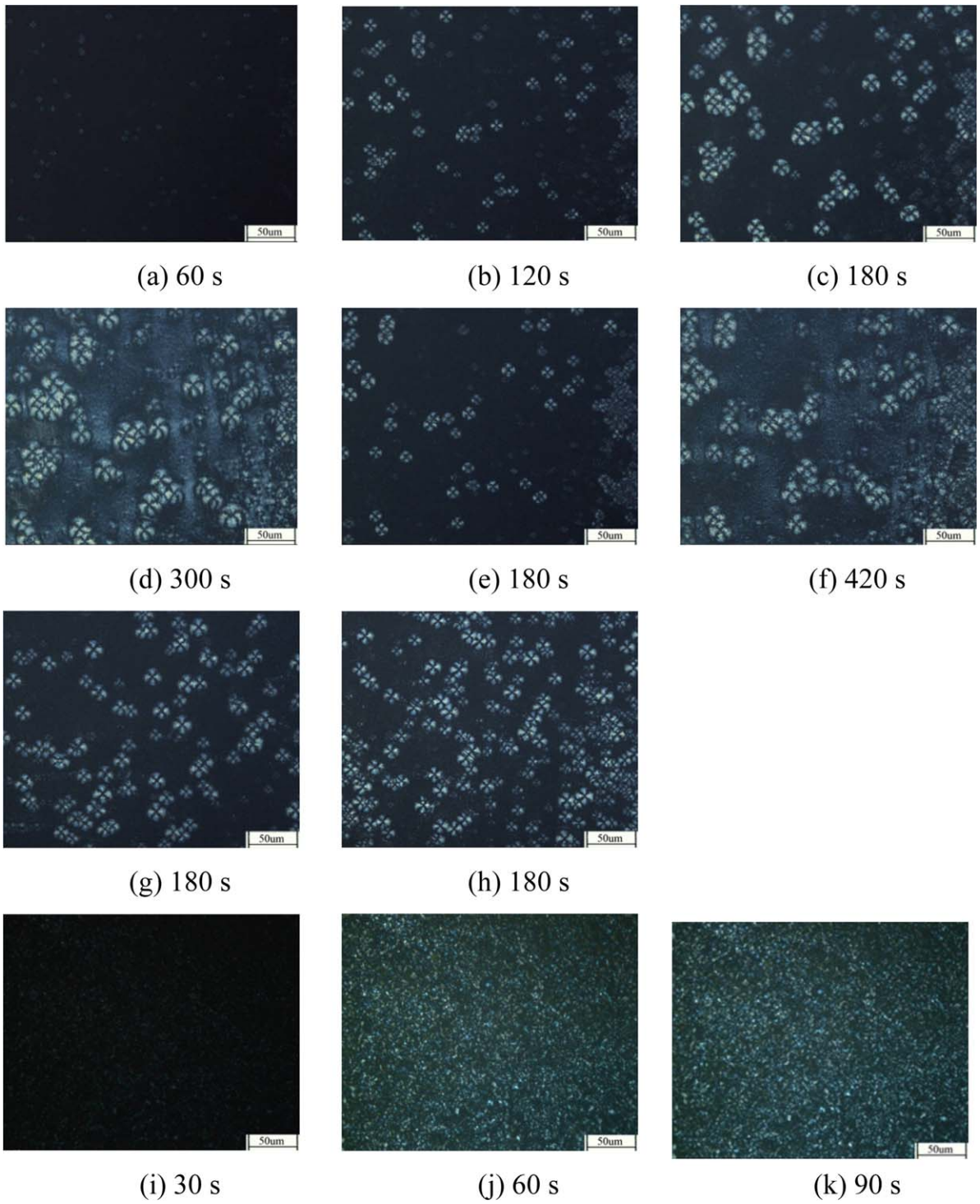

Figure 6. The time evolution of crystal morphologies with polarized optical microscope for PET isothermal crystallization at 220°C in (**a–d**) 230°C in (**e**, **f**), 215°C in (**g**) and 210°C in (**h**), respectively. PET/SMA3 ionomer isothermal crystallization at 220°C in (**i–k**). [Color figure can be viewed in the online issue, which is available at wileyonlinelibrary.com.]

and the final spherulite diameter at which crystals stop growing increases with increasing crystallization temperature. In particular, the nucleation sites are almost unchanged during the spherulite growth at the same view field of microscope for isothermal crystallization at 230°C, shown in Figure 6(e,f). This indicates that nucleation type of PET is heterogeneous nucleation controlled at higher crystallization temperatures due to the remaining catalyst or impurities as heterogeneous nucleation agents. For homogeneous nucleation, nucleation occurs spontaneously and randomly and thus nucleation sites are randomly

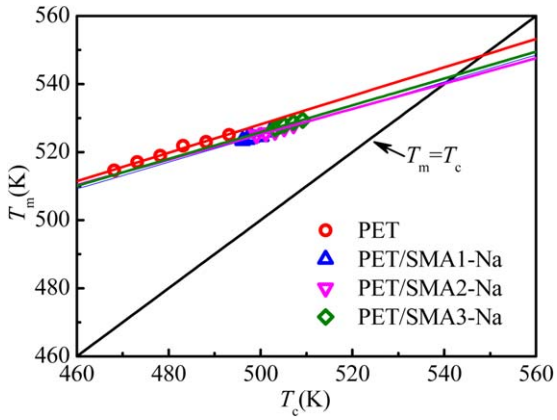

Figure 7. Hoffman–Weeks plots of the melting temperature T_m versus T_c for PET and PET/SMA ionomers to determine the equilibrium melting temperature T_m^0. [Color figure can be viewed in the online issue, which is available at wileyonlinelibrary.com.]

distributed. Comparing the results of isothermal crystallization at the same microscopic view field at relatively lower temperature such as 215°C and 210°C in Figure 6(g,h) as that of 230°C in Figure 6(f), the number of spherulites increases with decreasing the temperature although there are still some spherulites sites unchanged. This reflects that both homogeneous and heterogeneous nucleation occur for PET in relatively low crystallization temperature. Since the homogeneous nucleation barrier is intrinsic characteristics of polymers, increasing the supercooling degree will initiate the large driving force for the formation of homogeneous nuclei.[43] The crystallites of a stable phase need to exceed a critical size in order to develop a new phase according to the classical nucleation concept. In contrast, for heterogeneous nucleation, the critical size is not influenced by the temperature at large supercooling degree since the critical nucleus cannot be smaller than the molecular scale.[44] Figure 6(i–k) show that the spherulite size of PET sharply decreases with the addition of SMA3 ionomers. We note that SMA1 and SMA2 (not shown here) exhibit the same behavior as SMA3.

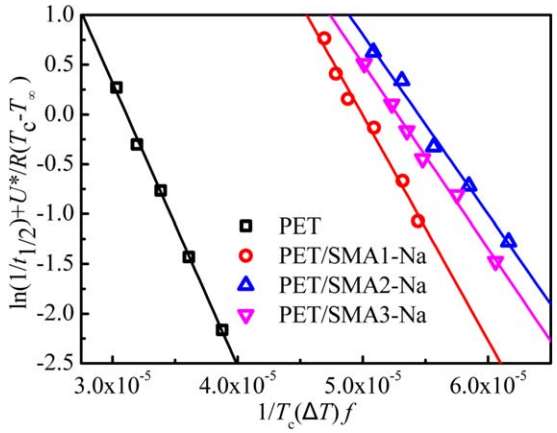

Figure 8. Lauritzen–Hoffman plots of $\ln\left(\frac{1}{t_{1/2}}\right)+\frac{U^*}{R(T_c-T_\infty)}$ versus $1/(T_c\Delta Tf)$ for isothermal crystallization of PET and PET/SMA ionomers. [Color figure can be viewed in the online issue, which is available at wileyonlinelibrary.com.]

This indicates that SMA ionomers provide a large number of nucleation sites, which increase the density of nucleus and thus accelerating the crystallization rate of PET.

The final spherulite crystal size of PET obtained by isothermal crystallization at a specific temperature depends on the density of nuclei. Due to introduction of a large number of nuclei by adding SMA ionomers, the spherulite crystals in PET/SMA ionomers samples instantaneously grow and subsequently are limited to grow due to impingement of adjacent spherulites. Therefore, Avrami exponents and the spherulite diameter decreased. Moreover, Avrami exponents are non-integer in our experiments. This was explained by Long et al.[45] who stated that the true nucleation rate and growth rate ρ_c/ρ_1 (where ρ_c and ρ_1 are the crystal and liquid densities, respectively) will change during the process of crystallization.

The Fold Surface Free Energy Based on the Hoffman–Lauritzen Theory

For polymer crystallization, the driving force mainly comes from the internal energy generated from the excess of thermodynamic free energy in the system, which comes from the transport of the molecules from the disordered liquid phase (melt or solution) to the ordered solid phase (crystal), and from the rotation and rearrangement of the molecules at the surface of the crystal.[45] Based on the classical thermodynamic concept of nucleation by Gibbs theory[46] and Turnbull and Fisher theory,[47] Hoffman and Lauritzen obtained the spherical crystal growth rate G as follows.[40,45]

$$G=G_0\exp\left(-\frac{U^*}{R(T_c-T_\infty)}\right)\exp\left(-\frac{K_g}{T_c\Delta T_f}\right) \quad (5)$$

$$f=2T_c/\left(T_m^0+T_c\right) \quad (6)$$

$$\Delta T=T_m^0-T_c \quad (7)$$

$$T_\infty=T_g-C \quad (8)$$

$$K_g=zb\sigma\sigma_e T_m^0/(\Delta H_f k_B) \quad (9)$$

where G_0 is a temperature-independent pre-exponential term, U^* is the activation barrier to transport molecules from the melt to the crystal surface equaling to 6284 J/mol.[48] R is the universal gas constant. T_c is the crystallization temperature. T_∞ is the temperature below which the transport ceases. K_g is the nucleation parameter. ΔT is the supercooling degree in eq. (7). f is an approximate correction factor, taking into account the fact that the fusion changes with supercooling. T_m^0 is the equilibrium melting temperature. T_g is the glass transition temperature. C is usually treated as an adjustable parameter at about 30°C derived experimentally.[45] z depends on the crystallization regimes of PET[45] with the value of 4 for crystallization regime I and III, and 2 for regime II. b is the monomolecular layer thickness, taken from the perpendicular separation of (0 1 0) planes, which is 5.53 Å.[49] σ is the side surface free energy of polymer crystal and σ_e is the fold surface free energy. ΔH_f is the enthalpy of fusion per unit volume with the value of 2.1×10^8 J/m^3.[49] k_B is the Boltzmann constant.

In order to obtain the fold surface free energy in the polymer crystallization process, the equilibrium melting temperature T_m^0 is needed to calculate the supercooling degree. Hoffman and

Table IV. Parameters Obtained from DSC Experimental Data According to Hoffman and Lauritzen Treatment for PET and PET/SMA Ionomers

	PET	PET/SMA1-Na	PET/SMA2-Na	PET/SMA3-Na
K_g (K^2)	2.85×10^5	2.26×10^5	1.80×10^5	1.86×10^5
σ_e (mJ/m^2)	110.6	44.4	35.5	36.4

Weeks plots[50] are often used to determine T_m^0 based on the observed linear relation between the melting temperature T_m and T_c. T_m can be obtained by reheating the crystallized samples at a rate of 10°C/min. The intersection point of the linear extrapolation of T_m versus T_c where $T_m = T_c$ is T_m^0. The equilibrium melting temperature T_m^0 corresponds to the melting temperature of the extended-chain crystals with infinite thickness, which should be independent of whether the nucleation agent is added or not. According to plots of T_m versus T_c, shown in Figure 7, the value of T_m^0 for PET is 548.39 K, which is close to the value of 547.15 K reported in the literature.[51] The calculated values of T_m^0 for PET with SMA ionomers are about 540 K, which shows a slight decrease compared with PET. We suppose that this discrepancy is in the range of extrapolated errors based on different isothermal crystallization temperature ranges selected for studying the isothermal crystallization kinetics of PET and PET with nucleation agent, although T_m^0 of PET decreased by nucleation agent was reported by the literatures.[16,52]

The crystallization half-time $t_{1/2}$ can also be used to represent the crystallization rates at different temperatures, which was proposed by Chan and Isayev.[53] Equation (5) can be rewritten as:

$$\frac{1}{t_{1/2}} = \frac{1}{(t_{1/2})_0}\exp\left(-\frac{U^*}{R(T_c - T_\infty)}\right)\exp\left(-\frac{K_g}{T_c \Delta T f}\right) \tag{10}$$

where $1/(t_{1/2})_0$ is a temperature-independent prepositional factor. Plots of $\ln\left(\frac{1}{t_{1/2}}\right) + \frac{U^*}{R(T_c - T_\infty)}$ versus $\frac{1}{T_c \Delta T f}$ for isothermal crystallization of PET and PET/SMA ionomers shown in Figure 8 can provide the nucleation parameters K_g (the negative value of the slope of the fitting line) according to eq. (10) and the values are listed in Table IV. From Figure 8, there is no obvious change in the slope of each curve in our examined temperature ranges, showing no change of the crystallization regime. The values of $\sigma\sigma_e$ can be calculated from eq. (9), where z is related to crystallization regimes of PET. According to the literature, PET crystallization kinetics follows regime I at high crystallization temperature (above 490 K), and the value of z is 4. The crystallization kinetics of PET/SMA ionomers samples in this work belongs to this regime. While the crystallization temperature is below 490 K, the regime II is operative and the value of z is 2. The crystallization kinetics of PET sample belongs to this regime. Next, combining eqs. (9) and (11), we obtain eq. (12) to calculate the fold surface free energy σ_e.

$$\sigma = \alpha \Delta H_f (a_0 b_0)^{1/2} \tag{11}$$

$$\sigma_e = \frac{K_g}{T_m^0} \frac{k_B}{z b \alpha (a_0 b_0)^{1/2}} \tag{12}$$

where α is derived experimentally to be 0.11 by analyzing the known behavior of hydrocarbons.[49] The unit cell dimensions, a_0 and b_0 for PET are 4.57 and 5.95 Å,[54] respectively. The σ_e values calculated from eq. (12) are listed in Table IV. The σ_e value of PET is in agreement with the previous references.[49] σ_e is also an important parameter to characterize the crystallization rate of polymers. The smaller the fold surface energy, the faster the crystallization rate of polymers. The addition of SMA ionomers can lower the fold surface free energy thus improving the crystallization rate of PET. Moreover, the fold surface free energy decreases with increasing the content of MA in SMA

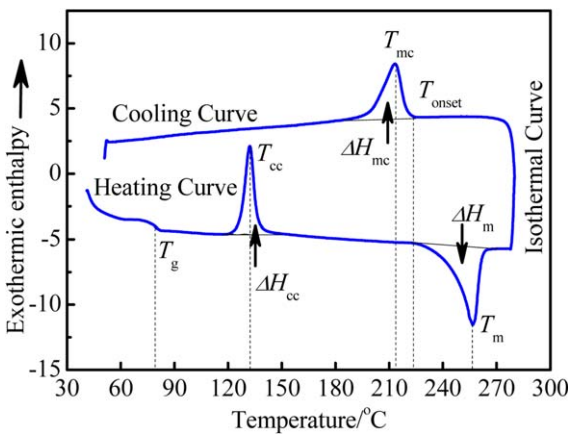

Figure 9. Typical heating and cooling DSC curves for PET. [Color figure can be viewed in the online issue, which is available at wileyonlinelibrary.com.]

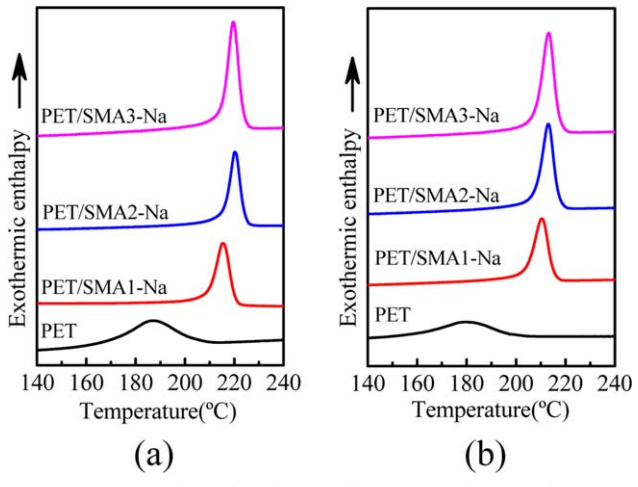

Figure 10. Non-isothermal melt-crystallization exotherms of PET and PET/SMA ionomers at two cooling rates: (**a**) 5°C/min; (**b**) 10°C/min. [Color figure can be viewed in the online issue, which is available at wileyonlinelibrary.com.]

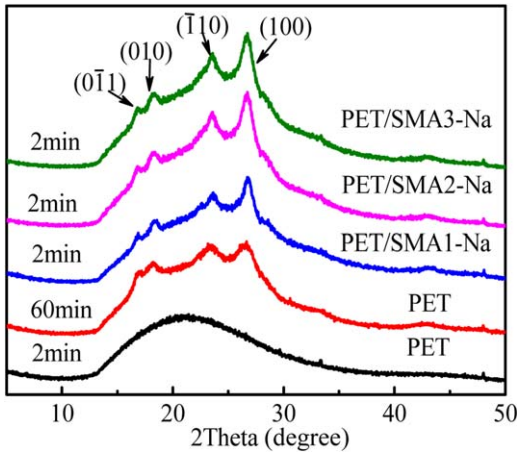

Figure 11. XRD patterns of PET and PET/SMA ionomers samples isothermally crystallized at 220°C. [Color figure can be viewed in the online issue, which is available at wileyonlinelibrary.com.]

copolymers, indicating that MA improves the compatibility between PET and SMA.

Non-Isothermal Crystallization Behaviors of PET and PET/SMA Ionomers

The studies of crystallization under isothermal conditions can be used directly to understand the mechanism of nucleation process and determine the crystallization rate of polymers. It is known that crystallization occurs when cooling from the melt or heating from the glassy state. In fact, non-isothermal crystallization is more practical in polymer processing. Therefore, it is necessary to analyze the non-isothermal crystallization behavior in order to design optimum processing condition for obtaining products with excellent properties. Figure 9 shows a typical heating and cooling DSC curve for PET. T_g is the glass transition temperature, T_{cc} is the cold crystallization temperature, ΔH_{cc} is the enthalpy of cold crystallization, T_m is the melting temperature, ΔH_m is the enthalpy of fusion, T_{onset} is the onset crystallization temperature on cooling process, T_{mc} is the melt-crystallization temperature and ΔH_{mc} is the enthalpy of melt-crystallization, $W_{1/2mc}$ is the half width of exothermal peak, which can reflect the crystallization rate. The narrower half width of exothermal peak indicates the faster the crystallization rate.

Figure 10 shows non-isothermal melt-crystallization exotherms and the parameters extracted from Figure 10 are listed in Table V for PET and PET/SMA ionomers at two different cooling rates. As clearly shown in Figure 10 and Table V, the values of T_{onset} and T_{mc} shift to higher temperature with the addition of SMA ionomers compared with PET and the higher content of MA, the higher temperature of T_{onset} and T_{mc} at the same cooling rate. The trends are the same as the case of isothermal crystallization. The half width of exothermal peak of samples also becomes narrow with the addition of SMA ionomers. These results confirm that the incorporation of a small amount of SMA ionomers such as 1 wt % can accelerate the crystallization rate of PET and hence acting as the nucleating agent for PET. The nucleating ability is ranked as SMA2 $\approx$ SMA3 $>$ SMA1, with the same trend of isothermal crystallization discussed above. Table V lists the degree of crystallinity of samples, which was determined by comparison of the apparent enthalpies with those of a 100% crystalline PET of 120 J/g according to the report by Roberts.[55] The results indicate that SMA ionomers increase the degree of crystallinity of PET at the same cooling rate.

Crystal Structure of PET and PET/SMA Ionomers by XRD Measurements

The characteristic X-ray peaks for both PET and PET/SMA ionomers occur at diffraction angles 2θ of about 15°–30°, corresponding to Figure 11. It is clear that, no peak is observed for PET film held at 220°C for 2 min. Whereas, XRD results of PET with SMA ionomers as nuclearing agents show that the crystallites are well formed referring to the powder diffraction file (PDF) and previous references.[49,56–58] These results further confirm that the addition of a small quantity of SMA ionomers indeed accelerates the crystallization of PET.

According to the above DSC results, provided that the samples were held at 220°C for above 60 min, fully-crystallized PET can be obtained. From Figure 11, comparing XRD results of the fully crystallized PET and PET/SMA ionomers samples, it is evident that the main peak positions do not shift at the same 2θ degree. Based on the Bragg formula, the interplanar crystal spacing can be calculated, which is 3.32, 3.74, 4.82, and 5.22 Å, respectively, corresponding to triclinic crystal form.[54,57] The lattice parameters are calculated as a=4.54Å, b=5.92Å, c=10.77Å, α=99.92°, β=

Table V. Non-Isothermal Crystallization Parameters Based on Different Cooling Rate Curves

Samples	Φ^a °C/min	T_{onset} °C	T_{mc} °C	$W_{1/2mc}$ °C	ΔH_{mc} J/g	$X_{DSC}{}^b$ %
PET	5	204.9	186.8	21.9	36.1	30.1
	10	198.5	179.6	25.6	34.5	28.8
PET/SMA1-Na	5	220.3	215.4	6.5	49.2	41.0
	10	215.3	210.5	6.6	39.9	33.3
PET/SMA2-Na	5	224.2	220.2	4.9	51.1	42.6
	10	217.2	213.1	5.6	43.6	36.3
PET/SMA3-Na	5	223.7	219.6	5.1	50.6	42.2
	10	217.4	213.2	5.7	42.1	35.1

[a] Cooling rate.
[b] Crystallinity extent. ΔH_m^0=120J/g.

118.22° and γ=111.37°. Furthermore, the degree of crystallinity (X_c) for each sample is estimated from the following eq. (13):[59]

$$X_c = \frac{\int_{2\theta_1}^{2\theta_2} I_c(2\theta)d(2\theta)}{\int_{2\theta_1}^{2\theta_2} I_c(2\theta)d(2\theta) + \int_{2\theta_1}^{2\theta_2} I_a(2\theta)d(2\theta)} \times 100\% \quad (13)$$

where the values of $2\theta_1$ and $2\theta_2$ used in this study are 10° and 40°, respectively. $I_c(2\theta)$ is the diffraction intensity from the crystalline phase, and $I_a(2\theta)$ is the diffraction intensity from the amorphous phases. $I_c(2\theta)$ is evaluated by using the annealed samples at the crystallization temperature. $I_a(2\theta)$ is evaluated by using the melt-quenched (amorphous) samples. Curves fitting and background subtracted XRD curves were performed via Origin software. The values of crystallinity are 25.9%, 34.5%, 40.9%, and 41.0% for PET, PET/SMA1-Na, PET/SMA2-Na, and PET/SMA3-Na samples, respectively, which is almost the same as above DSC results. This indicates that the crystallinity of PET is improved by the addition of SMA ionomers. Therefore, the addition of SMA ionomers does not change the crystal structure (still triclinic crystal), but improves the crystallization rate and decreases the spherulite size.

CONCLUSIONS

SMA ionomers with different molecular weight and mole ratios of MA and styrene were synthesized and designed as nucleation agents for improvement of PET crystallization. Compared with homogeneous nucleation, the heterogeneous nucleation is prone to occur at lower supercooling degree. New nucleation sites are created inside the PET matrix due to the introduction of only 1 wt % SMA ionomers, which leads to the change of nucleation type and decrease of the spherulite size thus promoting the crystallization rate of PET. The results also show that the effect of SMA ionomers as nucleation agent for PET have little relationship with the molecular weight and PDI of SMA ionomers. However, SMA2 and SMA3 copolymers with high content of MA have a better compatibility with PET matrix than SMA1 copolymer, thus improving the nucleation effect of SMA ionomers. As nucleation agent for PET, the nucleating ability is ranked as SMA2 $\approx$ SMA3 $>$ SMA1. Although the crystallization rate and crystallinity of PET is improved by SMA ionomers, the crystal structure is almost unchanged. In general, we conclude that SMA alternative ionomers synthesized in our experiments can act as effective nucleation agents during the crystallization process of PET. A systematic study of SMA block ionomers as nucleation agent is in progress. All the evidences confirm that enough nucleation sites and excellent compatibility between nucleation agent and the matrix are necessary requirements for the effective nucleation agent. This work provides a fresh idea to develop new nucleation agents for other polymers in the future.

ACKNOWLEDGMENTS

We thank financial support from the National Basic Research Program of China (Grant No. 2011CB605700). Funds from the NSF of China (Grant Nos. 21374023 and 91127033) are also acknowledged.

REFERENCES

1. Antoniadis, G.; Paraskevopoulos, K. M.; Vassiliou, A. A.; Papageorgiou, G. Z.; Bikiaris, D.; Chrissafis, K. *Thermochim. Acta* **2011**, *521*, 161.
2. Ge, C. H.; Shi, L. Y.; Yang, H.; Tang, S. F. *Polym. Compos.* **2010**, *31*, 1504.
3. Durmus, A.; Ercan, N.; Soyubol, G.; Deligoz, H.; Kasgoz, A. *Polym. Compos.* **2010**, *31*, 1056.
4. Zheng, K.; Yao, X. Y.; Chen, L.; Tian, X. Y. *J. Macromol. Sci., Phys.* **2009**, *48*, 318.
5. Tang, S.D.; Z. Xin. *Polymer* **2009**, *50*, 1054.
6. Ito, K.; Haraguchi, Y.; Hayakawa, S.; Toda, A. *Polym. J.* **2008**, *40*, 992.
7. Tianbin, W.; Yangchuan, K. *Eur. Polym. J.* **2006**, *42*, 274.
8. Natu, A. A.; Lofgren, E. A.; Jabarin, S. A. *Polym. Eng. Sci.* **2005**, *45*, 400.
9. Legras, R.; Dekoninck, J. M.; Vanzieleghem, A.; Mercier, J. P.; Nield, E. *Polymer* **1986**, *27*, 109.
10. Yu, H. M.; Han, K. Q.; Yu, M. H. *J. Appl. Polym. Sci.* **2004**, *94*, 971.
11. Garcia, D. *J. Polym. Sci., Part B: Polym. Phys.* **1984**, *22*, 2063.
12. Xu, Y. D.; Shen, Z. H.; Fan, X. H.; Zhou, Q. F. *Acta. Polym. Sin.* **2011**, *9*, 1053.
13. Wunderlich, B. Macromolecular Physics, Vol. 2 Crystal Nucleation, Growth, Annealing; Academic Press: New York, **1976**.
14. Legras, R.; Mercier, J.P.; Nield, E. *Nature* **1983**, *304*, 432.
15. Hwang, S. Y.; Im, S. S. *Polym. Compos.* **2011**. *32*, 259.
16. Jiang, X. L.; Luo, S. J.; Sun, K.; Chen, X. D. *Express Polym. Lett.* **2007**, *1*, 245.
17. Aharoni, S. M. *J. Appl. Polym. Sci.* **1984**, *29*, 853.
18. Wittmann, J. C., Lotz, B. *J. Polym. Sci. Part B: Polym. Phys.* **1981**, *19*, 1837.
19. Wittmann, J. C., Lotz, B. *J. Polym. Sci. Part B: Polym. Phys.* **1981**, *19*, 1853.
20. Binsbergen, F. L. *Polymer* **1970**, *11*, 253.
21. Cheng, S. Z. D.; Li, C. Y.; Zhu, L. *Eur. Phys. J. E.* **2000**, *3*,195.
22. Inoue, M. *J. Polym. Sci., Part A: General Papers*, **1963**, *1*, 2013.
23. Legras, R.; Bailly, C.; Dekoninck, J. M.; Mercier, J. P.; Nield, E. *Polym. Mater. Sci. Eng.* **1984**, *50*, 495.
24. Kalfoglou, N. K.; Skafidas, D. S. *Eur. Polym. J.* **1994**, *30*, 933.
25. Yu, Y.; Yu, Y. L.; Jin, M.; Bu, H. S. *Macromol. Chem. Phys.* **2000**, *201*, 1894.
26. Yu, Y.; Bu, H. S. *Macromol. Chem. Phys.* **2001**, *202*, 421.
27. Ramesan, M. T.; Lee, D. S. *Iran. Polym. J.* **2008**, *17*, 281.
28. Berti, C.; Celli, A.; Colonna, M.; Fiorini, M.; Marianucci, E. *J. Macromol. Sci., Phys.* **2003**, *42*, 989.
29. Zhang, H. S.; Zhang, Y.; Guo, W. H.; Xu, D. D.; Wu, C. F. *J. Appl. Polym. Sci.* **2008**, *109*, 3546.

30. Yoon, K. H.; Lee, H. W.; Park, O. O. *J. Appl. Polym. Sci.* **1998**, *70*, 389.
31. Yoon, K. H.; Lee, H. W.; Park, O. O. *Polymer* **2000**, *41*, 4445.
32. Karakus, G.; Yenidunya, A. F.; Zengin, H. B.; Polat, Z. A. *J. Appl. Polym. Sci.* **2011**, *122*, 2821.
33. Saad, G. R.; Morsi, R. E.; Mohammady, S. Z.; Elsabee, M. Z. *J. Polym. Res.* **2008**, *15*, 115.
34. Butler, G. B.; Do, C. H.; Zerner, M. C. *J. Polym. Sci., Part A: Polym. Chem.* **1989**, *A26*, 1115.
35. Ha, N. T. H. *Polymer* **1999**, *40*, 1081.
36. Lessard, B.; Maric, M. *Macromolecules* **2010**, *43*, 879.
37. Avrami, M. *J. Chem. Phys.* **1939**, *7*, 1103.
38. Avrami, M. *J. Chem. Phys.* **1941**, *9*, 177.
39. Ergoz, E.; Fatou, J. G.; Mandelkern, L. *Macromolecules* **1972**, *5*, 147.
40. Mandelkern, L. Crystallization of Polymers; Cambridge University: New York, **2004**.
41. Booth, A.; Hay, J. N. *Polymer* **1971**, *12*, 365.
42. Chew, S.; Griffiths, J. R.; Stachurski, Z. H. *Polymer* **1989**, *30*, 874.
43. Massa, M. V.; Dalnoki-Veress, K. *Phys. Rev. Lett.* **2004**, *92*, 255509.
44. Woo, E.; Huh, J.; Jeong, Y. G.; Shin, K. *Phys. Rev. Lett.* **2007**, *98*, 136103.
45. Long, Y.; Shanks, R. A.; Stachurski, Z. H. *Prog. Polym. Sci.* **1995**, *20*, 651.
46. Gibbs, J. W. The Collected Works; Longmans, Green: New York, **1928**.
47. Turnbull, D.; Fisher, J. C. *J. Chem. Phys.* **1949**, *17*, 71.
48. Hoffman J. D.; Davis, G. T.; Lauritzen J. I. In Treatise on Solid State Chemistry; Hannay, N. B., Ed; Plenum Press: New York, **1976**; Vol. *3*.
49. Lu, X. F.; Hay, J. N. *Polymer* **2001**, *42*, 9423.
50. Hoffman, J. D.; Weeks, J. J. *J. Res. Nat. Bur. Stand. Sec. A-Phys. Chem.* **1962**, *66*, 13.
51. Reinsch, V. E.; Rebenfeld, L. *J. Appl. Polym. Sci.* **1994**, *52*, 649.
52. Deshpande, V. D.; Jape, S. *J. Appl. Polym. Sci.* **2010**, *116*, 3541.
53. Chan, T. W.; Isayev, A. I. *Polym. Eng. Sci.* **1994**, *34*, 461.
54. Yamashit,Y. *J. Polym. Sci., Part A: General Papers* **1965**, *3*, 81.
55. Roberts, R. C. *Polymer* **1969**, *10*, 113.
56. Keum, J. K.; Jeon, H. J.; Song, H. H.; Choi, J. I.; Son, Y. K. *Polymer* **2008**, *49*, 4882.
57. Bai, C.; Spontak, R. J.; Koch, C. C.; Saw, C. K.; Balik, C. M. *Polymer* **2000**, *41*, 7147.
58. Daubeny, R. d. P.; Bunn, C. W. *Proc. R. Soc. London, Ser. A, Math. Phys. Sci.* **1954**, *226*, 531.
59. Marubayashi, H.; Asai, S.; Hikima, T.; Takata, M.; Iwata, T. *Macromol. Chem. Phys.* **2013**, *214*, 2546.